Journal of Radioanalytical and Nuclear Chemistry (2021) 328:941–950
https://doi.org/10.1007/s10967-021-07715-x

Investigation of neutron shielding materials for low-background gamma spectrometry

Abdul J. Khan[1] · Xin Li[1,2] · Douglas K. Haines[1] · Timothy J. Hoffman[1] · Thomas M. Semkow[1,2]

Received: 8 December 2020 / Accepted: 5 April 2021 / Published online: 27 April 2021

Abstract
In gamma spectrometers located at ground-level or in shallow-underground laboratories, muon-induced neutrons contribute significantly to the background. We studied several neutron-shielding materials including water, pure polyethylene (PPE), borated polyethylene (BPE) and lithiated polyethylene (LPE) positioned inside the lead shield. Neutrons are scattered and absorbed inside these materials, however, sequential (n,n′γ), (n,γ) and (n,α) reactions generate gamma emissions. The resulting background increased by 35.9% for water and 37.6% for PPE. For BPE, the background increased by 11.3% only and it decreased by 9.4% for LPE, owing to the absorption of neutrons by boron and lithium, respectively.

Keywords Muon-induced neutron · Borated polyethylene · Lithiated polyethylene · Plastic scintillator · Adhesive sealant

Introduction

Low-background gamma spectrometry with high-purity germanium detectors has been widely applied to monitoring natural radionuclides such as ^{226}Ra, ^{228}Ra as well as anthropogenic radionuclides such as fission products in the environment for contamination control and nonproliferation applications. A significant usage of low-background gamma spectrometry has been in fundamental physics experiments such as neutrino oscillation, $0\nu\beta\beta$ decay, and dark matter search [1–10]. Gamma spectrometry has the advantages that samples can be measured non-destructively, without preconcentration during sample preparation, and that multiple emission lines can be detected simultaneously for the determination of multiple radionuclides. With particular combination of detector efficiency, sample quantity, and counting time, the lower the background of the germanium detector is, the lower the detection limit can be achieved.

The background in high-purity germanium (HPGe or Ge) gamma spectrometer originates mainly from the radiations of cosmic rays, activated radioisotopes in the germanium crystal and copper cryostat, as well as the natural radionuclides in the environment, shielding, and detector components. An additional background can originate from the electronic or microphonic noise. There is a marked difference between ground-level or shallow-underground locations and deep-underground locations of gamma spectrometers in terms of muon flux. While the muons can be discriminated electronically, the secondary processes induced by muons are significant sources of background at ground-level and shallow locations. These processes are considerably diminished or can be neglected deeply underground owing to the muon flux drop off.

The particles and interactions involved in cosmic rays are described in Fig. 1. Primary (galactic) cosmic rays, originating outside the Earth's atmosphere, are composed of protons (about 95%, depending on energy), alpha particles (4%) and heavy ions (≈ 1%) [11]. They interact with nitrogen, oxygen, and argon in the atmosphere resulting in a cascade of hadrons including primary neutrons and pions. A neutral pion decays to two photons with a mean lifetime of 85 as, while a charged pion decays to a muon and a neutrino or antineutrino with a lifetime of about 26 ns. Depending on the charge, muon decays to an electron plus an electron antineutrino and a muon neutrino, or a set of their anti-particles, with a lifetime of about 2.2 μs [11]. To project main features

Deceased: Xin Li.

✉ Abdul J. Khan
abduljabbar.khan@health.ny.gov

[1] Wadsworth Center, New York State Department of Health, Empire State Plaza, Albany, NY 12237, USA

[2] Department of Environmental Health Sciences, School of Public Health, University at Albany, State University of New York, Rensselaer, NY 12144, USA

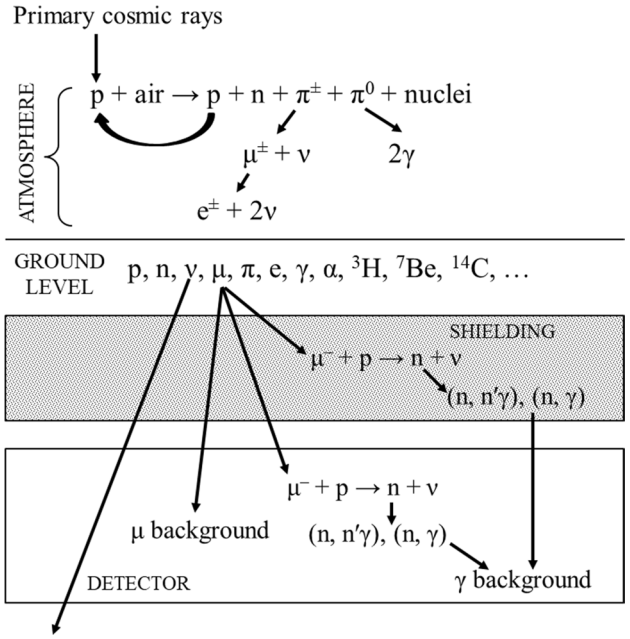

Fig. 1 The composition of cosmic rays and the interactions with the atmosphere, shielding materials, and in the germanium detector

in Fig. 1, we do not separate different neutrino flavors as well as antineutrinos from neutrinos and use the symbol ν in general. In the secondary cosmic rays at the ground level, neutrinos have very small cross section with the shielding and detector materials, and almost leave no signal in the relatively small Ge detector. Charged particles, neutrons, and gamma rays are mostly stopped by the shielding materials such as lead, steel, concrete, and overburden. However, muons have a strong penetrating power to travel through the shielding and generate a continuous smooth background plus a pronounced muon-induced annihilation peak on the detector, unless the detector is located deep underground to have the muon flux reduced by several orders [11].

The components of the muon background in the detector include direct ionization, δ-electron production, electron–positron pair production, muon decay, and muon bremsstrahlung: their contributions vary with muon energy [12]. Moreover, muons interact with the protons in the nuclei of detector and shielding materials in a process of muon capture generating high-energy secondary neutrons [13]. The secondary neutrons interact with the detector and shielding materials through elastic (n,n′) and inelastic (n,n′γ) neutron scattering until they are slowed down, followed by neutron capture and activation (n,γ) and, to a lesser extent (n,α) and (n,f) reactions, resulting in the gamma background at surface or shallow-underground laboratories [1, 14–17]. Usually, the muon background and prompt gamma emissions following muon-induced neutron activation events can be significantly rejected by a muon veto detector, but still there remain considerable delayed gamma emissions from neutron-activated isotopes with half-lives of milliseconds or longer, which contribute significantly to the background. This background can be verified by direct irradiating of a HPGe detector with neutrons [18]. Therefore, neutron shielding becomes an important component to further reduce the background of gamma spectrometers located at ground level or shallow underground, like our laboratory.

Various neutron shielding materials have been used for the applications in nuclear power plants, waste storage sites, medicine, fundamental research, oil exploration, and other fields. Concrete is one such material used for shielding because of its cost-effectiveness, structural flexibility, and good shielding performance for both neutron and gamma radiation. Doping materials such as boron, colemanite mineral, and polyethylene (PE) can be added into concrete to further improve its neutron shielding performance [19, 20]. When optical transparency for visible light and consistency in the density and composition are required, glass attracts more attention. Among different oxide glasses, boron oxide shows excellent abilities as both glass former and neutron absorber [21].

Considering both neutron shielding efficiency and mechanical properties, boron-containing composites are developed for nuclear industry, such as boron nitride particles in high density polyethylene polymer matrix [22].

In gamma spectrometry measurements and particle physics experiments, pure polyethylene (PPE) [5, 23], sometimes doped with boron (BPE) [8, 10] or lithium (LPE), have been applied as neutron shielding materials.

In PE-based shielding, neutrons are scattered by hydrogen and carbon nuclei, and lose energy during collisions. Meanwhile, neutrons may be absorbed by hydrogen or the doping elements such as boron and lithium, which have high cross-section for thermal neutron capture. After capturing a free neutron, the system is at an unstable state, which may de-excite by emitting a gamma photon such as

$$^{1}\mathrm{H} + \mathrm{n} \rightarrow {}^{2}\mathrm{H} + \gamma(2223\,\mathrm{keV}), \tag{1}$$

or split to two particles such as

$$^{10}\mathrm{B} + \mathrm{n} \rightarrow {}^{4}\mathrm{He} + {}^{7}\mathrm{Li} + \gamma(478\,\mathrm{keV}), \tag{2}$$

and

$$^{6}\mathrm{Li} + \mathrm{n} \rightarrow {}^{7}\mathrm{Li} \rightarrow {}^{4}\mathrm{He} + {}^{3}\mathrm{H}. \tag{3}$$

The cross-sections for the above processes depend on neutron energy. For thermal neutrons (0.0253 eV), the cross sections for reactions in Eqs. 1 through 3 are 0.333, 3840, and 938 b (barns), respectively [24]. Therefore, the effects of different shielding materials on the detector background may vary significantly. It is important to understand their shielding mechanisms and effects for an appropriate design

of gamma spectrometry system. In this work, we systematically studied the effects of several commonly used neutron shielding materials including water, PPE, BPE, and LPE, on the detector background, using our low-background gamma spectrometry system [25, 26]. Since the cosmic neutrons inducing gamma background are produced in the lead shield close to the germanium detector and the detector itself, we are interested in the effects of the studied materials positioned close to the detector, and not outside of the lead shield.

Natural radiation background has been studied in a variety of sealants [27, 28]. One reason for sealants is to prevent radon leakage for radium analysis by gamma spectrometry [29, 30]. Another is to protect the detector system from radon and thoron daughters. In this work we tested two sealants for natural radionuclide levels. The selected sealants were at the extremes of adhesion: the sealant with strong adhesion to prevent sample leak, as well as a sealant with low adhesion which can be easily peeled off enabling reusing of the sample and container.

Materials and methods

Nuclear Chemistry Laboratory (NCL), Wadsworth Center, has been involved in ultra-low background gamma spectrometry for several years [6, 25, 26]. The laboratory is located under the 47-floor Corning Tower which provides an overburden of 31 m-water-equivalent (mwe) shielding and reduces the cosmic-ray muon flux by a factor of 3 at angles between 0° and 45° from zenith. Moreover, a 15.2-cm (6-in.) thick steel room made from pre-World War II steel is installed at NCL to shield the detectors from environmental gamma rays from the building construction materials. A diagram of the spectrometer is shown in Fig. 2. The lead shielding includes three layers from the outside to the inside: 7.6-cm (3-in.) of low-background lead (^{210}Pb concentration 20 Bq/kg; Boliden, Stockholm, Sweden), 3-in. of very low-background lead (^{210}Pb < 3 Bq/kg and ^{40}K < 1 mBq/kg; Plombum Firma-Laboratorium, Kraków, Poland), and a 2-cm thick insert of ultra-pure Alpha-Lo lead (α-flux 7×10^{-4} counts/hour · cm^2 and K impurity 0.01 ppm; Pure Technologies, Tequesta, FL, USA). The lead shielding is surrounded by seven 5.1-cm (2-in.) thick plastic scintillators (Model BC-408, Saint-Gobain Crystals, Newbury, OH, USA), as the muon veto detectors, which cover nearly 4π angle for the HPGe detector in the center. The HPGe detector used for gamma spectrometry has a 2.682-kg germanium crystal with a relative efficiency of 140% at 1332-keV ^{60}Co peak (Model GX13023; Mirion Technologies (Canberra), Inc., Meriden, CT, USA). The detector has a copper cryostat and a thin carbon window on the top of end cap, which extends the useful gamma energy range down to 10 keV. The sample space inside the lead shield is continuously flushed with liquid nitrogen boil-off. With all the passive and active shielding, the background is reduced to 0.91 counts/min · kg Ge in the energy range of 50–2700 keV, which allows us to quantitatively study the effects of various types of neutron shielding materials with high accuracy. This system compares well with the world lowest background gamma spectrometers [7].

The water measured for comparison was distilled, deionized, and completely filled a nominal 800-mL Marinelli beaker for counting [31]. The Marinelli beaker was positioned on a stand made of polymethyl methacrylate (PMMA). The PMMA stand was kept inside the lead

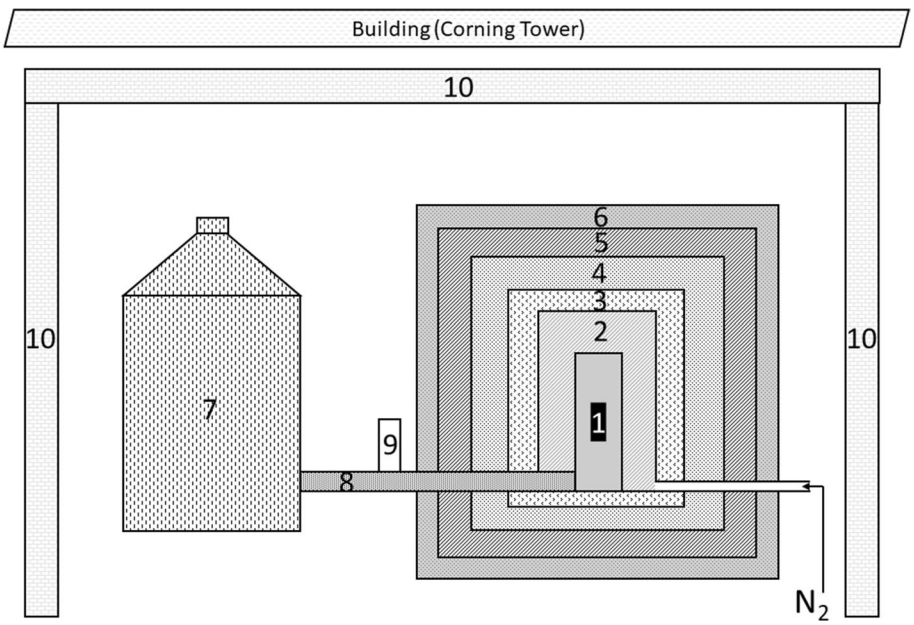

Fig. 2 The diagram of the ultra-low background gamma spectrometer showing various components and shielding materials (the dimensions are not to scale). 1: Ge detector, 2: testing materials, 3: Alpha-Lo lead, 4: Plombum lead, 5: Boliden lead, 6: plastic scintillators, 7: Dewar, 8: cryostat, 9: preamplifier, 10: steel room

shielding during the study, even in the measurement of the background spectrum, to ensure consistency when comparing the investigated materials.

The PPE, BPE and LPE were manufactured by Shieldwerx [32]. The Model SWX-201 BPE has 5% boron by weight, which consists of 19.6% ^{10}B and 80.4% ^{11}B. The total density is 0.95 g/cm^3. The weight percentage of Li in Model SWX-215 LPE is 7.5%, consisting of 92.6% ^{7}Li and 7.4% ^{6}Li, with a density of 1.06 g/cm^3. The PPE was the material used for the above two products without doping. The three types of PE, obtained as 9″ × 9″ × 1″ sheets, were machined into discs and small blocks. The blocks were stacked around the detector below and onto the PMMA stand. The disks were positioned on the top of stacked blocks without touching the detector. The space abbreviated with number 2 in Fig. 2 was nearly filled with the PE materials.

Another aspect of low-level gamma spectrometry is to prevent contamination of detectors from either samples or from radioactive standards leakage. It was observed that screw caps as well as snap-on lids often develop leaks. Therefore, an additional sealing by commercially available adhesive sealants is necessary to prevent spillage and contamination of detectors. Adhesive sealants are also used to stop the diffusion of radon gas from the containers for radium analysis. We studied two commercially available adhesive sealants on the extreme sides of adhesion. One was Flex Glue, a silicone-rubber type of strong adhesion (Swift Response, Weston, FL, USA). Another sealant studied was Phenoseal Vinyl Adhesive Caulk (Phenomenal Brands, Phenoseal Products, a division of DAP Products Inc., Baltimore, MD, USA) which possesses low-adhesion property and is thus easily removable. The adhesive sealants were filled into a nominal 300-mL plastic container and allowed to cure. The HPGe detector has a delicate carbon window on the top of end cap, which is held by a copper ring above it. The containers were rested on this ring, without touching the carbon window.

The data acquisition was performed using Lynx Digital Signal Analyzer and Genie 2000 Gamma Acquisition and Analysis software (Mirion Technologies (Canberra), Inc., Meriden, CT, USA). Most of the gamma spectra, including the background, were acquired for 16.3 days each, except that water was measured for 13.9 days and PPE for 14.1 days.

Results and discussion

The gamma-ray spectra were analyzed using Mirion/Canberra VMS Standard Peak Search algorithm. This algorithm fits the gamma peaks using the Gunnink and Niday step-function model for the baseline under the peak [33], which has been revised in Ref. [34]. By selecting the highest search sensitivity, most peaks can be fitted automatically. For a few weaker peaks, a version of this algorithm in the Mirion/Canberra Interactive Peak Fit was applied, where the user can fix peak range and/or position. Using known compilations to assign detected peaks in the gamma-ray spectra [35–37], series of characteristic gamma peaks were identified. The information about the resolved gamma peaks and their assignment is listed in Table 1. Only a few peaks could not be resolved by these methods, abbreviated in Table 1 as "none".

The uncertainties of the peak areas are larger than from the Poisson statistics because of subtraction of the background under the peak and are calculated by the Mirion/Canberra software. In our data, the 1-sigma uncertainties typically range between 10 and 50% and are occasionally larger for weak peaks. The uncertainties were not reported in Table 1 because they were not used in subsequent analysis. The peak areas divided by the live time resulted in the counting rates (counts/day) that are given in Table 1 to accuracy of two decimal figures, even if not always supported by the uncertainties. In statistical evaluation of the data it is proper practice not to truncate intermediate values because it can significantly affect the accuracy of the final result. The data in Table 1 are intermediate and they sum up to the final values in Table 2 as described below. This is the reason for keeping several significant digits in Table 1.

The background of the gamma spectrometer is depicted in Fig. 3. In addition to muon-induced continuum, the peaks identified in the spectrum, as shown in Fig. 3, can be classified into four categories: natural-series radionuclides such as ^{214}Pb or ^{208}Tl, from the uranium and thorium series, respectively; primordial ^{40}K; neutron-activated radioisotopes such as ^{71}Ge and ^{71m}Ge plus the 511-keV annihilation peak, and characteristic X-rays. We have excluded from further analysis several weak peaks seen in Fig. 3, such as the 1120-keV peak from ^{214}Bi.

The first and second peak categories come from the manufacturing of detector and shielding components, and they can be reduced by material purification, but will not be improved by neutron shielding. The third category involves the elements in the detector such as germanium crystal and copper in the cryostat, or in the lead shielding. They are activated to excited states through neutron scattering and neutron capture, and then de-excite by emitting prompt or delayed gamma rays. Usually, the delayed gamma rays from metastable states have lower energies ($\leq$200 keV) and prompt gamma emissions have higher energies (> 200 keV). One can see a clear peak at 2223 keV in Fig. 3b, which is due to the thermal neutron capture of ^{1}H (Eq. 1) from the hydrogen present in the PMMA stand. The aim of adding neutron shielding materials is to reduce the neutron flux, and consequently, neutron capture and scattering events. Accordingly, the background contribution from the third category

Table 1 Counting rates (counts/day) of the resolved peaks from tested neutron-shielding materials

Peak	Assignment[1]	Energy (keV)	Background	Water	PPE	BPE	LPE
1	^{70}Ge(n,γ)^{71m}Ge	23.4	15.97	19.80	19.26	2.33	4.11
2	^{210}Pb	46.5	2.64	4.90	6.73	4.30	5.47
3	^{72}Ge(n,γ)^{73m}Ge	53.4	16.58	28.58	18.69	6.45	9.58
4	^{234Th}	63.3	19.77	24.62	31.51	32.05	17.50
5	^{72}Ge(n,γ)^{73m}Ge	66.7	131.66	174.89	168.03	60.30	124.04
6	Bi K_α X-rays	74.8	8.60	11.45	8.78	9.33	5.40
		77.1	7.06	7.85	7.65	10.01	9.46
7	^{234}Th	92.6	18.97	18.86	19.76	23.15	24.26
8	^{74}Ge(n,γ)^{75m}Ge	139.7	59.99	93.82	84.47	40.90	49.68
9	^{76}Ge(n,γ)^{77m}Ge	159.7	16.21	22.03	22.02	6.82	11.54
10	^{70}Ge(n,γ)^{71m}Ge	175.0	10.32	12.60	10.83	0.43	4.48
11	^{235}U	185.7	28.80	23.83	24.85	20.39	25.42
	^{226}Ra	186.2					
12	^{70}Ge(n,γ)^{71m}Ge	198.4	61.65	103.46	90.42	33.47	56.25
13	^{212}Pb	238.6	17.07	14.33	17.21	22.35	20.51
14	^{214}Pb	242.0	6.82	4.82	5.17	7.61	5.96
15	^{74}Ge(n,γ)^{75}Ge	253.2	6.94	9.29	10.48	1.35	3.75
16	^{63}Cu(n,γ)^{64}Cu	278.3	16.52	26.78	23.37	7.68	16.09
	^{65}Cu(n,2n)^{64}Cu						
17	^{214}Pb	295.2	7.86	6.77	9.20	14.49	12.40
18	^{72}Ge(n,γ)^{73}Ge	325.7	9.58	13.03	11.12	3.19	3.93
	^{70}Ge(n,γ)^{71}Ge	326.8					
19	^{228}Ac	338.3	3.25	3.10	7.22	9.46	4.67
20	^{63}Cu(n,γ)^{64}Cu	343.9	5.10	8.35	8.14	2.15	2.15
	^{65}Cu(n,2n)^{64}Cu						
21	^{214}Pb	351.9	16.83	20.88	17.84	25.67	23.33
22	^{10}B(n,α)^{7}Li	477.6	None	None	4.32	333.69	5.90
23	^{70}Ge(n,γ)^{71}Ge	499.9	7.12	11.23	11.47	3.32	4.54
24	Annihilation	511.0	61.53	89.93	89.01	33.10	46.85
25	^{208}Tl	583.2	3.93	3.53	3.04	7.74	7.06
26	^{73}Ge(n,γ)^{74}Ge	595.9	14.06	21.60	20.11	4.67	7.37
27	^{214}Bi	609.3	21.06	21.82	24.00	21.49	20.63
28	^{228}Ac	911.2	3.87	5.98	5.24	9.33	4.42
29	^{228}Ac	969.0	2.27	2.30	2.83	5.53	2.58
30	^{40}K	1460.8	22.90	20.95	18.27	21.80	26.16
31	^{214}Bi	1764.5	3.62	3.31	3.89	3.99	4.05
32	^{1}H(n,γ)^{2}H	2223.3	3.32	36.29	53.96	3.19	7.18
33	^{208}Tl	2614.5	2.89	3.24	2.55	4.11	4.18

[1]Metastable (^{m}) isotopes are defined with half-lives of 1 ns or longer; prompt gamma emissions are from the excited states with half-lives shorter than 1 ns [30]

can be reduced. The annihilation is mainly caused by cosmic muons, muon-induced fast neutrons, and high energy gamma rays. Among them, neutron shielding may reduce the contribution of neutron-induced annihilation events. The characteristic X-rays from muon interactions in the Pb shielding are significantly reduced by muon veto shielding, because they are prompt events. Therefore, the X-rays seen in Fig. 3a are primarily Bi X-rays from the decay of natural $^{212, 214}$Pb radionuclides.

The gamma-ray spectra with various neutron sensitive materials were analyzed as described above and the peak counting rates in counts/day are listed in Table 1. The data demonstrate that the counting rates of the nuclides from the same category have similar trends among the investigated materials. To illustrate this, we selected three regions of interest depicted in Figs. 4 and 5, including several representative peaks (Fig. 4a: ^{71}Ge and ^{73}Ge at 326 keV, ^{228}Ac at 338 keV, ^{64}Cu at 344 keV, and ^{214}Pb at 352 keV; Fig. 4b:

Table 2 Comparison of the background levels among various materials studied

Background	Water	PPE	BPE	LPE	Flex Glue	Phenoseal
Material						
Sample mass (kg)						
None	0.778	2.199	2.749	2.650	0.215	0.308
Total counting rate 50–2700 keV (counts/min · kg Ge)						
0.91	1.24	1.26	1.02	0.83	1.07	1.25
Deviation from background spectrum (%)						
Total counting rate	35.9	37.6	11.3	−9.4	16.6	36.6
Natural series	3.6	13	32	13	3.1	92
^{40}K	−8.5	−20	−4.8	14	−6.5	4.2
Activation plus 511-keV	54	48	24	−18	26	8.6

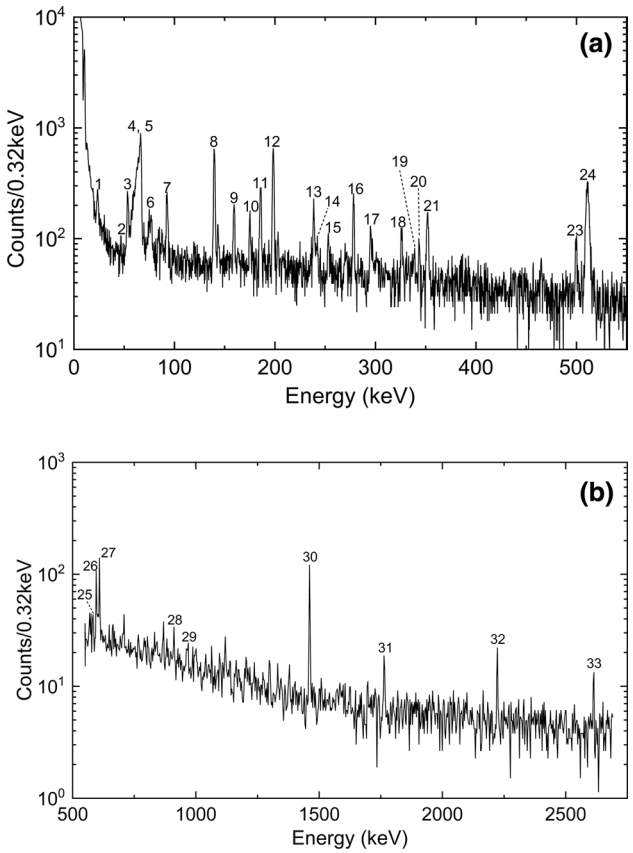

Fig. 3 The background spectrum measured in the ultra-low background gamma spectrometer for 16.3 days except PPE for 14.1 days: **a** 0–550 keV region, **b** 550–2650 keV region. Peaks are numbered according to Table 1

^{2}H at 2223 keV; and Fig. 5: 478-keV peak from ^{7}Li, ^{71}Ge at 500 keV, and 511-keV annihilation peak) covering the aforementioned categories one and three of background contributions.

The total background counting rates in the range 50–2700 keV (in counts/min · kg Ge) are given in Table 2 for each investigated material, as well as their % deviations from the background spectrum. For the total counting rates, we rounded the values up to two decimal figures, and their deviations from background to 1 decimal figure. In both cases, the number of significant digits are supported by the large number of counts in the total spectra.

In addition, for each investigated material, peak counting rates from Table 1 were summed up for each category of background: natural series, K-40, and activation plus 511-keV, and are given in Table 2 as % deviation from those of the background spectrum. These deviations are rounded up to two significant digits, reflecting the uncertainties of individual counting rates in Table 1. Also given in Table 2 are the masses of investigated materials.

The background from the natural series radionuclides is mainly due to impurities in the detector and shielding, which may depend on the original concentration or may be introduced in manufacturing. As shown in Fig. 4a, the ^{214}Pb peak at 352 keV has the lowest intensity in the background spectrum, and it becomes more pronounced in the spectra of PPE, BPE, and LPE. The same phenomenon can be noticed for the 338-keV ^{228}Ac peak, with weaker intensities. The counting rates from other natural series radionuclides listed in Table 1 also demonstrate the same trend among the PE materials. The sum of natural series in water is increased only by 3.6% from the background and much more in PE materials (Table 2). This indicates that the PE materials were not made ultra-pure, but that the inner lead shielding has higher purity.

The background trend for ^{40}K, which exists naturally but has different chemical behavior, is quite different from that for the natural series. The counting rates of ^{40}K for water, PPE, and BPE are actually lower than for the background spectrum (Table 2). Since these materials effectively surround the Ge detector, the lowering of potassium background may be due to its origin in the lead shielding and some attenuation of potassium gamma rays by the investigated materials. On the contrary, the ^{40}K activity increased in LPE (Table 2). This can be explained by the fact that Li in LPE and K are homologs in the periodic table, having

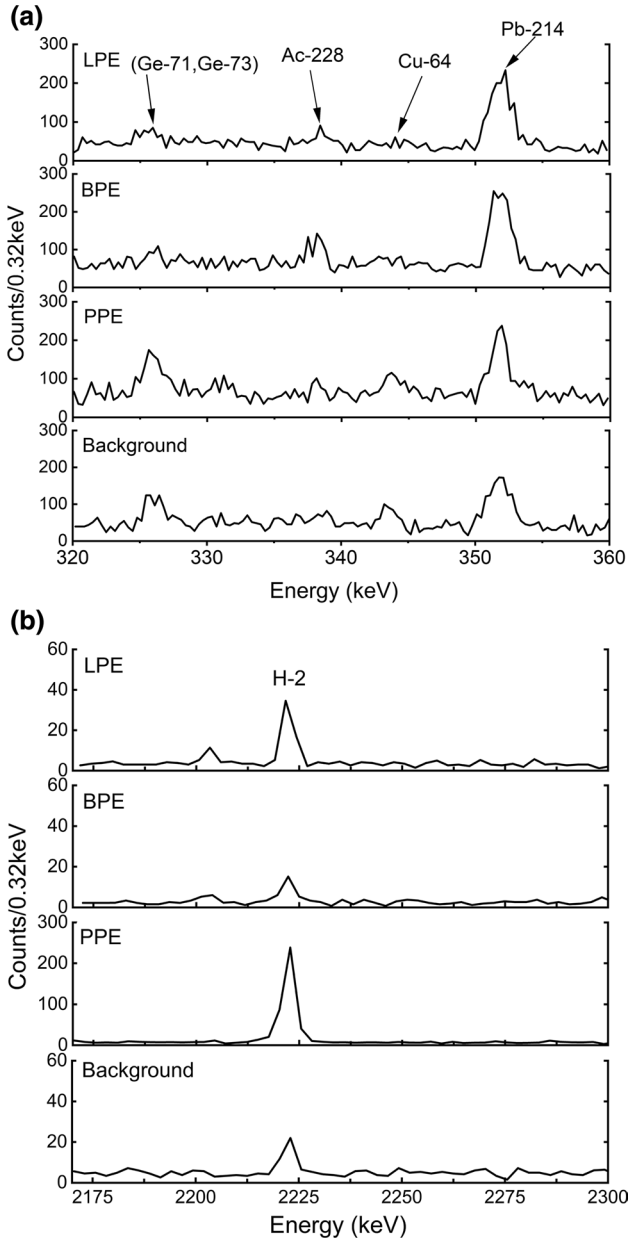

Fig. 4 **a** The gamma spectra in the regions of 320–360 keV, and **b** around 2223-keV peak, for LPE, BPE, and PPE materials, as well as background, measured for 16.3 days, except PPE for 14.1 days

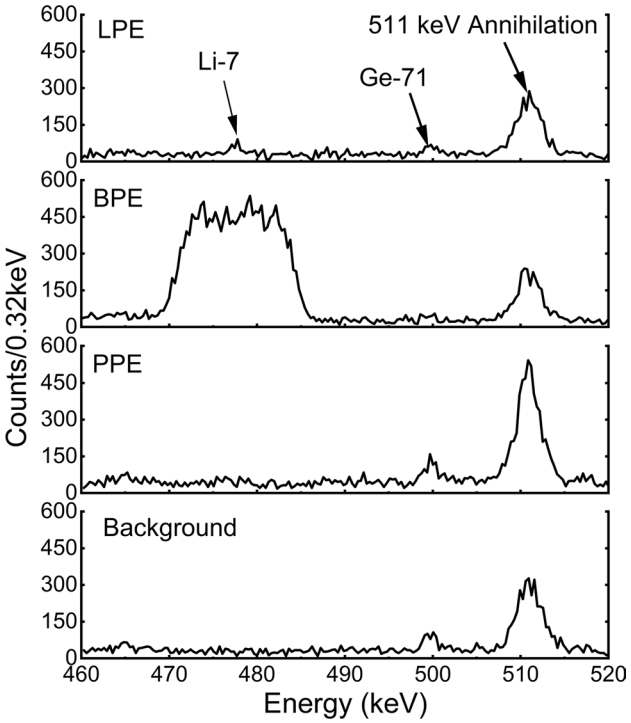

Fig. 5 The gamma spectra in the region of 460–520 keV, for LPE, BPE, and PPE materials, as well as background, measured for 16.3 days, except PPE for 14.1 days

similar chemical behavior. Since LPE is not an ultra-pure material, it may be slightly contaminated with ^{40}K.

The spectra of water and PPE are similar to each other, and the only difference is that water sample contains less impurities than PPE from natural decay series (to simplify, only the spectrum of PPE is plotted in the Figs. 4, 5). The reason is that water and PPE have similar ^{1}H-rich components (H_2O and $(CH_2)_n$, respectively) and the same dominant mechanism of the interaction with neutron (elastic scattering). They both behave as a neutron moderator. Generally, the cross-section of neutron capture increases when neutrons slow down. The cross section for thermal neutron (n,γ) is 0.333 b [24]. Therefore, the muon-induced neutrons are scattered in water and PE shielding, and while the neutron flux may be reduced, the slowed neutrons activate more materials around the detector as the result. The contributions from neutron-activated radioisotopes and neutron-induced annihilation are remarkably increased in PPE and water as compared with the background, which is indicated by the enhancement of ^{71,73}Ge prompt gamma peaks at 326 keV (Fig. 4a), ^{1}H neutron capture gamma peak at 2223 keV (Fig. 4b), as well as ^{71}Ge 500-keV prompt gamma and the 511-keV annihilation peaks (Fig. 5). It is also implied as a slightly elevated baseline of the PPE spectrum, which is the Compton continuum from high-energy prompt gamma rays. It can be seen from Table 1 that the counting rate of 2223 keV in the spectrum of PPE is increased more than water (53.96 vs. 36.29 counts/day), because the PPE sample contains a larger quantity of hydrogen. Overall, rather than reduce the background, water and PPE shielding cause more gamma emissions and the total background level is increased to 1.24 and 1.26 counts/min · kg Ge, respectively, which is 35.9% more for water and 37.6% more for PPE than the background (see Table 2).

BPE contains ^{10}B in the boron doping with its natural abundance. ^{10}B has a large (n,α) (Eq. 2) cross section (3840

b for thermal neutrons [24]) and absorbs neutrons considerably. From Fig. 5, the ^{71}Ge 500-keV peak and 511-keV annihilation peak are reduced, and so are the 326-keV and 344-keV peaks in Fig. 4a from activated germanium and copper isotopes, as well as 2223-keV peak from hydrogen in Fig. 4b; all as compared with PPE and background. The same trend can be seen for the other peaks in the category of neutron-activated isotopes listed in Table 1. Therefore, BPE is used for neutron shielding in experiments [8, 10]. However, the product nucleus ^{7}Li de-excites (Eq. 2) and emits strong 478-keV gamma photons as seen in Fig. 5. Due to the light mass of ^{7}Li, the peak shows significant Doppler broadening [38, 39]. The 478-keV peak is strong enough that its Compton scattering elevated the spectrum baseline in lower energy range, as seen in Fig. 4a. The 478-keV peak total contribution overcomes the reduction of the neutron activation peaks (since there are less neutrons) in the spectrum and causes the total background counting rate increase by 11.3% with respect to the background, although it is lower than the background for either water or PPE (see Table 2). Therefore, BPE is usually not located next to the detector but has extra lead or copper shielding in between [8].

In LPE, ^{6}Li absorbs neutron through (n,t) reaction and results in an α particle, as seen in Eq. 3. The advantage is that there is no gamma emission from the products of this reaction. Although the (n,t) cross section of ^{6}Li (938 b for thermal neutrons [24]) is smaller than that of ^{10}B, it still depresses the flux of neutrons significantly, and the total background level is reduced by 9.4%, as seen in Table 2. As shown in the figures, the peaks of ^{71}Ge and 511-keV annihilation in LPE are lower than of the background, but higher than those of BPE. ^{2}H peak intensity is between those for BPE and PPE. A very small peak at 478 keV is also seen in the spectrum of LPE (Fig. 5), which may be due to the de-excitation of ^{7}Li, following the (n,γ) reaction of ^{6}Li and (n,n′) reaction of ^{7}Li in the doping. Apparently, the 478-keV level in ^{7}Li is less populated in these reactions than in that for ^{10}B given in Eq. 2.

The results of the gamma analysis for adhesive sealants are also presented in Table 2, although we did not provide individual peak counting rates in Table 1 for brevity. To facilitate further discussion, we note that the masses of sealants are approximately 5 to 10 times smaller than the masses of water and PE materials. The counting rate from the natural series radionuclides has increased by 3.1% for Flex Glue and 92% for Phenoseal (Table 2). Considering the mass difference, Flex Glue appears to be material of similar radiopurity to PE materials, however Phenoseal is significantly less clean than all other materials investigated. This is even seen in the ^{40}K background which decreased in Flex Glue, similarly to water, PPE, and BPE, whereas it increased for Phenoseal. On the contrary, the activation plus 511-keV have increased more in Flex Glue than in Phenoseal, possibly due to the effect of silicon, present in Flex Glue, on neutron activation.

The two opposite effects of higher natural background in Phenoseal and higher activation background in Flex Glue, resulted in a total background increase by 16.6% in Flex Glue and by 36.6% in Phenoseal, the effect also partially caused by higher mass of Phenoseal (Table 2). Therefore, while Flex Glue has lower background than Phenoseal, both have significantly higher specific background than water or PE materials. These facts make the adhesives, particularly Phenoseal, less suitable in ultra-low background applications. In some low-background applications they may be useful because the mass required to seal a typical container is very small.

Conclusions

We investigated the effects of various neutron sensitive materials on the germanium detector background, including water, PPE, BPE, and LPE, using our ultra-low background gamma spectrometer. The goal was to elucidate if the materials can decrease neutron-induced background in ground-level or shallow-underground gamma spectrometry applications, as well as to determine their radiopurity. The PE materials were industry standard pure materials and our efforts to secure ultra-pure materials were unsuccessful. The measurements show that the PPE, BPE, and LPE are not ultra-pure, and there is slight increase in the background from environmental radionuclides. Water and PPE elevate the background due to neutron moderation and enhanced neutron scattering and activation. BPE absorbs neutrons significantly, but the total background still increases because of the gamma emission from the (n,α) reaction of ^{10}B. Only LPE decreased the total background by 9.4% owing to clean neutron absorption via (n,t) reaction of ^{6}Li. Therefore, if one uses BPE as neutron shielding, an extra inner layer of lead or copper must be applied to shield the sequential gamma emission as has been done before [8], while LPE can be placed near the detector for background reduction. A neutron absorber containing Li isotopically enriched with ^{6}Li would be a good direction of study to improve neutron shielding in low-background applications at ground-level or shallow-underground laboratories.

We also studied purity of two adhesive sealants: Flex Glue of strong adhesion and Phenoseal of weak adhesion. It was found that that Flex Glue has contamination level from natural radioactivity similar to that of the PE materials, while Phenoseal was considerably more contaminated. However, neutron activation is significantly higher in Flex Glue than in Phenoseal. These sealants can still be used in some low-background applications since the mass required to seal counting container is very small.

Acknowledgement Thanks are due to Brian McDermott and Donald Hanna for valuable discussion on neutron shielding.

References

1. Heusser G (1995) Low-radioactivity background techniques. Annu Rev Nucl Part Sci 45:543–590. https://doi.org/10.1146/annurev.ns.45.120195.002551
2. Povinec PP, Comanducci JF, Levy-Palomo I (2004) IAEA-MEL's underground counting laboratory in Monaco—background characteristics of HPGe detectors with anti-cosmic shielding. Appl Radiat Isot 61:85–93. https://doi.org/10.1016/j.apradiso.2004.03.019
3. Laubenstein M, Hult M, Gasparro J, Arnold D, Neumaier S, Heusser G, Köhler M, Povinec P, Reyss JL, Schwaiger M, Theodórsson P (2004) Underground measurements of radioactivity. Appl Radiat Isot 61:167–172. https://doi.org/10.1016/j.apradiso.2004.03.039
4. Aalseth CE, Bonicalzi RM, Cantaloub MG et al (2012) A shallow underground laboratory for low-background radiation measurements and materials development. Rev Sci Instrum 83(113503):1–10. https://doi.org/10.1063/1.4761923
5. Armengaud E et al (2013) (The EDELWEISS Collaboration) Background studies for the EDELWEISS dark matter experiment. Astropart Phys 47:1–9. https://doi.org/10.1016/j.astropartphys.2013.05.004
6. Khan AJ, Semkow TM, Beach SE, Haines DK, Bradt CJ, Bari A, Syed UF, Torres M, Marrantino J, Kitto ME, Menia T, Fielman E (2014) Application of low-background gamma-ray spectrometry to monitor radioactivity in the environment and food. Appl Radiat Isot 90:251–257. https://doi.org/10.1016/j.apradiso.2014.04.011
7. Cagniant A, Douysset G, Fontaine JP, Gross P, Le Petit G (2015) An introduction to γ^3 a new versatile ultralow background gamma spectrometer. Background description and analysis. Appl Radiat Isot 98:125–133. https://doi.org/10.1016/j.apradiso.2015.01.027
8. Heusser G, Weber M, Hakenmüller J, Laubenstein M, Lindner M, Maneschg W, Simgen H, Stolzenburg D, Strecker H (2015) GIOVE: a new detector setup for high sensitivity germanium spectroscopy at shallow depth. Eur Phys J C75(531):1–16. https://doi.org/10.1140/epjc/s10052-015-3704-2
9. Gastrich H, Gößling C, Klingenberg R, Kröninger K, Neddermann T, Nitsch C, Quante T, Zuber K (2016) The dortmund low background facility—low-background spectrometry with an artificial overburden. Appl Radiat Isot 112:165–176. https://doi.org/10.1016/j.apradiso.2016.03.025
10. Zeng Z, Mi Y, Ma H, Cheng J, Su J, Yue Q (2014) The characteristics of a low background germanium gamma ray spectrometer at China JinPing underground laboratory. Appl Radiat Isot 91:165–170. https://doi.org/10.1016/j.apradiso.2014.05.022
11. Patrignani C et al (2016) (Particle Data Group), Review of particle physics. Chin Phys C40(100001):1–1808. https://doi.org/10.1088/1674-1137/40/10/100001
12. Vojtyla P (1995) A computer simulation of the cosmic-muon background induction in a Ge γ-spectrometer using GEANT. Nucl Instrum Methods Phys Res B100:87–96. https://doi.org/10.1016/0168-583X(95)24900271-5
13. Charalambus S (1971) Nuclear transmutations by negative stopped muons and the activity induced by the cosmic-ray muons. Nucl Phys A 166:145–161. https://doi.org/10.1016/0375-9474(71)90419-2
14. Heusser G (1996) Cosmic ray interaction study with low-level Ge-spectrometry. Nucl Instrum Methods Phys Res A369:539–543. https://doi.org/10.1016/S0168-9002(96)80046-5
15. Jovančević N, Krmar M (2011) Neutrons in the low-background Ge-detector vicinity estimated from different activation reactions. Appl Radiat Isot 69:629–635. https://doi.org/10.1016/j.apradiso.2010.12.004
16. Mietelski JW (2019) Detection of background thermal neutrons in a modified low-background germanium gamma-ray spectrometer. J Radioanal Nucl Chem 322:1331–1339. https://doi.org/10.1007/s10967-019-06843-9
17. Baginova M, Vojtyla P, Povinec PP (2020) The neutron component of background of an HPGe detector operating in a surface laboratory. Appl Radiat Isot 166(109422):1–15. https://doi.org/10.1016/j.apradiso.2020.109422
18. Chao JH (1993) Neutron-induced gamma rays in germanium detectors. Appl Radiat Isot 44:605–611. https://doi.org/10.1016/0969-8043(93)90177-C
19. Oto B, Madak Z, Kavaz E, Yaltay N (2019) Nuclear radiation shielding and mechanical properties of colemanite mineral doped concretes. Radiat Eff Defects Solids 174:899–914. https://doi.org/10.1080/10420150.2019.1668390
20. DiJulio DD, Cooper-Jensen CP, Perrey H, Fissum K, Rofors E, Scherzinger J, Bentley PM (2017) A polyethylene-B_4C based concrete for enhanced neutron shielding at neutron research facilities. Nucl Instrum Methods Phys Res A859:41–46. https://doi.org/10.1016/j.nima.2017.03.064
21. Sayyed MI, Dong MG, Tekin HO, Lakshminarayana G, Mahdi MA (2018) Comparative investigations of gamma and neutron radiation shielding parameters for different borate and tellurite glass systems using WinXCom program and MCNPX code. Mater Chem Phys 215:183–202. https://doi.org/10.1016/j.matchemphys.2018.04.106
22. Zhang X, Zhang X, Guo S (2019) Simple approach to developing high-efficiency neutron shielding composites. Polym Eng Sci 59:E348–E355. https://doi.org/10.1002/pen.25065
23. Aprile E et al (2013) The neutron background of the XENON100 dark matter search experiment. J Phys G: Nucl Part Phys 40(115201):1–17. https://doi.org/10.1088/0954-3899/40/11/115201
24. Evaluated Nuclear Data File (ENSF), Brookhaven National Laboratory, Upton, NY, USA, https://www.nndc.bnl.gov/exfor/endf00.jsp. Accessed 2 Mar 2021
25. Semkow TM, Parekh PP, Schwenker CD, Khan AJ, Bari A, Colaresi JF, Tench OK, David G, Guryn W (2002) Low-background gamma spectrometry for environmental radioactivity. Appl Radiat Isot 57:213–223. https://doi.org/10.1016/S0969-8043(02)00085-4
26. Haines DK, Semkow TM, Khan AJ, Hoffman TJ, Meyer ST, Beach SE (2011) Muon and neutron-induced background in gamma-ray spectrometry. Nucl Instrum Methods Phys Res A652:326–329. https://doi.org/10.1016/j.nima.2011.01.137
27. Busto J, Gonin Y, Hubert F, Hubert Ph, Vuilleumier JM (2002) Radioactivity measurements of a large number of adhesives. Nucl Instrum Methods Phys Res A492:35–42. https://doi.org/10.1016/S0168-9002(02)01280-9
28. Parekh PP, Bari A, Semkow TM, Torres MA (2002) A new method for sealing containers with liquid samples for radioactivity measurements. J Radioanal Nucl Chem 253:321–325. https://doi.org/10.1023/A:1019626631694
29. Mauring A, Gäfvert T (2013) Radon tightness of different sample sealing methods for gamma spectrometric measurements of ^{226}Ra. Appl Radiat Isot 81:92–95. https://doi.org/10.1016/j.apradiso.2013.03.022
30. Bonczyk M, Samolej K (2019) Testing of radon tightness of beakers and different types of sealing used in gamma-ray spectrometry for ^{226}Ra concentration determination in NORM. J Environ Radioact 205–206:55–60. https://doi.org/10.1016/j.jenvrad.2019.05.007
31. IEEE standard techniques for determination of germanium semiconductor detector gamma-ray efficiency using a standard

Marinelli (reentrant) beaker geometry, ANSI/IEEE Standard 680–1978, The Institute of Electrical and Electronics Engineers, New York, NY, USA (1978)
32. Shieldwerx, a Division of Bladewerx LLC, Rio Rancho, NM, USA, http://www.shieldwerx.com/poly-based-shielding.html. Accessed 7 Dec 2020
33. Gunnink R, Niday JB (1972) Computerized Quantitative Analysis by Gamma-Spectrometry, Vol. I, Description of the Gamanal Program, Report UCRL-51061. Lawrence Livermore Laboratory, University of California, Livermore, CA
34. Semkow TM, Khan AJ, Menia TA, Li X, Chu LT, Torres MA, Bari A (2019). Detection limit for Ra-228 in drinking water by gamma spectrometry, in Detection Limits in Air Quality and Environmental Measurements, ed. M. J. Brisson. ASTM International, West Conshohocken, PA, 146–160. Doi: https://doi.org/10.1520/STP161820180060
35. Chart of Nuclides, National Nuclear Data Center, Brookhaven National Laboratory, Upton, NY, USA, https://www.nndc.bnl.gov/nudat2/. Accessed 7 Dec 2020
36. Gilmore GR (2008) Practical gamma-ray spectrometry. Wiley, Chichester
37. Choi HD et al (2007) Database of prompt gamma rays from slow neutron capture for elemental analysis, Publication STI/PUB/1263. International Atomic Energy Agency, Vienna
38. Tojo T (1971) Measurement of the Doppler broadening of gamma-ray energy with Ge(Li) detector. J Nucl Sci Technol 8:48–50. https://doi.org/10.1080/18811248.1971.9734772
39. Choi HD, Jung NS, Park BG (2009) Analysis of Doppler-broadened peak in thermal neutron induced $^{10}B(n, \alpha\gamma)^{7}Li$ reaction using HyperGam. Nucl Eng Technol 41:113–124. https://doi.org/10.5516/NET.2009.41.1.113